Conclusion

The preliminary results of the investigation of a plunging airfoil without dynamic stall have revealed several interesting features of the unsteady wake. The near wake consists of a laminar portion and a turbulent portion. The laminar portion is caused by the induced flow of the circulation around the airfoil. The magnitude of the velocity defect is less than 10% of the maximum velocity defect at the center of the wake, but the width is very large compared with the width of the turbulent portion. Thus, the streamwise momentum deficit of the laminar portion of the wake cannot be neglected. The simultaneous measured velocity traces and the Reynolds stress distribution indicate that the unsteady wake has quite different turbulent structures in the upper and lower parts of the wake. The mean transverse velocity was accurately measured. The variations in the circulation during a cycle of oscillation were then obtained by integrating the velocities around the plunging airfoil. The phase-averaged wake profiles are different at different phase angles due to the instantaneous changes in drag and momentum integral around the airfoil.

Acknowledgment

This work was supported by the U.S. Army Research Office under Contract No. DAAG-29-78-G-0073.

References

[1] McCroskey, W. J., "Recent Developments in Dynamic Stall," *Symposium on Unsteady Aerodynamics*, Vol. 1, Univ. of Arizona, March 1975, pp. 1-34.

[2] Fujita, H. and Kovasznay, L.S.G., "Unsteady Lift and Radiated Sound from a Wake Cutting Airfoil," *AIAA Journal*, Vol. 12, Sept. 1974, pp. 1216-1221.

[3] Ho, C. M. and Kovasznay, L.S.G., "Sound Generation by a Single Cambered Blade in Wake Cutting," *AIAA Journal*, Vol. 14, June 1976, pp. 763-766.

[4] Satyanarayana, B., "Unsteady Wake Measurements of Airfoils and Cascades," *AIAA Journal*, Vol. 15, May 1977, pp. 613-618.

[5] Ho, C. M. and Chen, S. H., "Unsteady Wake of a Plunging Airfoil," AIAA Paper 80-1446, Snowmass, Colo., July 1980.

AIAA 81-4301

Two-Dimensional Transonic Nozzle Flows with Shock

C.Q. Lin* and S.F. Shen†
Cornell University, Ithaca, N.Y.

Introduction

IN existing analytical studies of two-dimensional and axially-symmetric transonic nozzle flow problems (for example, see the survey paper of Hall and Sutton[1]), the presence of a shock has yet to be included in the representation. It is believed that, however specialized or limited in scope, such a solution should be valuable from both the basic viewpoint and as a check of various computational methods based upon discretization. The present Note gives an analytical treatment of two-dimensional nozzle flows with shock by expanding the perturbation velocity potential into a double power series. Specifically, an exact solution of the transonic small perturbation equation is continued across a given shock wave and the nozzle shape after the shock is determined as a consequence. Details are worked out for a parabolic shock. The tedious computation for the coefficients of the higher-order terms in the series is performed by computer. The accuracy of the series solution is assessed by evaluating the local residuals. The region of convergence is then considerably enlarged by using the Euler transformation on both coordinates. An illustrative numerical example is given.

Received Jan. 20, 1981; revision received April 13, 1981.

*Visiting Fellow; permanently, Professor, Northwestern Polytechnical University, Xi'an, China.

†Professor, Sibley School of Mechanical and Aerospace Engineering.

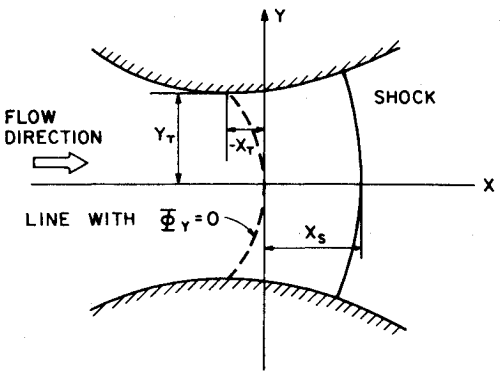

Fig. 1 Nozzle geometry and coordinate system.

Governing Equation and the Solution before the Shock

The Cartesian coordinate system (X, Y) is shown in Fig. 1. We consider a nozzle symmetrical about the X axis and the origin is taken at the sonic point. The transonic small perturbation equation is

$$a^*\Phi_{YY}=(\gamma+1)\Phi_X\Phi_{XX} \tag{1}$$

where Φ is the perturbation velocity potential, a^* the critical speed, and γ the ratio of specific heats. Before the shock, if the velocity along the X axis varies linearly with X, the exact solution of Eq. (1) is well known,[2]

$$\Phi=c\left\{\frac{1}{2}X^2+\frac{1}{2}(\gamma+1)\frac{c}{a^*}XY^2+\frac{1}{24}(\gamma+1)\frac{c^2}{a^{*2}}Y^4\right\} \tag{2}$$

where c is a constant specifying the amplitude of the perturbation velocity. The associated nozzle-wall shape satisfies the tangency condition

$$\frac{dY}{dX}=\frac{\Phi_Y}{a^*+\Phi_X} \tag{3}$$

Let the wall shape be expressed by the series

$$\bar{\eta}=b_0+\sum_{j=2}^{\infty}b_j\bar{\xi}^j \tag{4}$$

with

$$\bar{\xi}=\frac{cX}{a^*}+\frac{\gamma+1}{6}\left(\frac{cY}{a^*}\right)^2 \quad \text{and} \quad \bar{\eta}=(\gamma+1)\left(\frac{cY}{a^*}\right)^2 \tag{5}$$

The line $\bar{\xi}=0$, along which $\Phi_Y=0$, now passes through the throat position. The coefficient b_0 is related to the throat width Y_T, since at $\bar{\xi}=0$ in Eq. (4)

$$b_0=\bar{\eta}_T=(\gamma+1)(c^2Y_T^2/a^{*2}) \tag{6}$$

The recursion formula for the coefficients b_{j+1} $(j=1,2,3,\ldots)$ is omitted for brevity. The constant c and the radius of

curvature of the nozzle wall at the throat, R_T, are related by

$$\frac{R_T}{Y_T} = \frac{1}{3} + \frac{a^{*2}}{(\gamma+1)c^2 Y_T^2} \tag{7}$$

Solution behind a Parabolic Shock

Let X_s be the intersection of the shock with the X axis. For the solution behind the shock, the following nondimensional variables are introduced:

$$\Phi = cX_s^2\phi, \qquad X = X_s x, \qquad Y = X_s[(\gamma+1)K]^{-1/2} y \tag{8}$$

where $k = cX_s/a^*$ is a measure of the shock strength.

Assume next a parabolic shape for the shock

$$x + \lambda y^2 = 1 \tag{9}$$

where λ is determined by the orthogonality condition between the shock and the nozzle wall. For convenience, we use the transformed coordinates

$$\xi = x + \lambda y^2 - 1, \qquad \eta = y^2 \tag{10}$$

so that the parabolic shock coincides with $\xi = 0$. Equation (1) then becomes

$$\phi_\xi \phi_{\xi\xi} - 4\eta(\phi_{\eta\eta} + 2\lambda\phi_{\eta\xi} + \lambda^2\phi_{\xi\xi}) - 2(\phi_\eta + \lambda\phi_\xi) = 0 \tag{11}$$

The solution before the shock, Eq. (2), is now

$$\phi = \frac{1}{2} + \left(\frac{1}{2} - \lambda\right)\eta + \left(\frac{1}{24} - \frac{1}{2}\lambda + \frac{1}{2}\lambda^2\right)\eta^2 + \left[1 + \left(\frac{1}{2} - \lambda\right)\eta\right]\xi + \frac{1}{2}\xi^2 \tag{12}$$

The approximate shock conditions are, from p. 33 of Ref. 2,

$$\phi_{I,x} + \phi_{II,x} = 2\left(\frac{dx}{dy}\right)_s^2 \quad \text{and} \quad \phi_I = \phi_{II} \tag{13}$$

the subscripts I and II denoting the points on opposite sides of the shock. Expressing the solution behind the shock as a Taylor series in ξ

$$\phi = \sum_{j=0}^{\infty} f_j(\eta)\xi^j \tag{14}$$

we find from the shock conditions Eqs. (13)

$$f_0(\eta) = \frac{1}{2} + \left(\frac{1}{2} - \lambda\right)\eta + \left(\frac{1}{24} - \frac{1}{2}\lambda + \frac{1}{2}\lambda^2\right)\eta^2$$

$$f_1(\eta) = -1 - (\tfrac{1}{2} - \lambda - 8\lambda^2)\eta \tag{15}$$

Next, substitution of Eq. (14) into Eq. (11) gives the recursion formula for $f_j(\eta)$ $(j = 2,3,\ldots)$. For instance,

$$f_2(\eta) = \frac{(1-4\lambda) + (\tfrac{1}{2} - 11\lambda + 16\lambda^2 + 80\lambda^3)\eta}{2 + (1 - 2\lambda + 8\lambda^2)\eta} \tag{16}$$

The expressions for the rest of $f_j(\eta)$ are cumbersome. Instead, let us expand the functions $f_j(\eta)$ also into a Taylor series

$$f_j(\eta) = \sum_{k=0}^{\infty} a_{j,k}\eta^k \qquad (j = 0,1,2,\ldots) \tag{17}$$

The recursion formula for $a_{j,k}$ is straightforward to derive, again omitted here for brevity. A double Taylor series expression for function ϕ results finally from combining Eqs. (15) and (18). In actual computation, it is truncated into

$$\phi \doteq \sum_{j=0}^{2m+1} \sum_{k=0}^{m-[j/2]} a_{j,k}\xi^j\eta^k \tag{18}$$

where $[j/2]$ is the integer part of $j/2$. Equation (18) contains all terms which can be evaluated if the coefficients $a_{2,k}$ and $a_{3,k}$ are kept up to $k = m-1$.

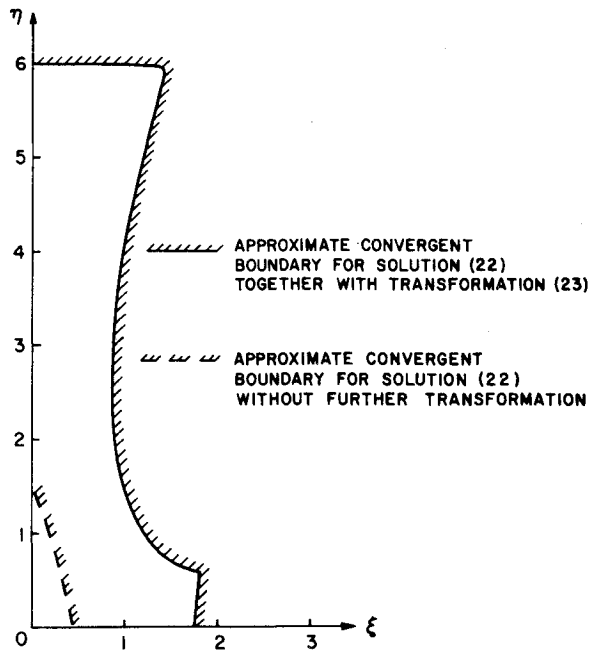

Fig. 2 Comparison of regions of convergence defined by $|\epsilon| \le 0.01$, for $R_T/Y_T = 5$, $K = 0.2$, $m = 9$.

Numerical Example and Improvement of the Series

Computations have been carried out for the case $R_T/Y_T = 5$, $K = 0.2$ and with $m = 9$ in Eq. (18). The accuracy of the truncated series representation is assessed by evaluating the residuals $\epsilon(\xi,\eta)$ from substituting Eq. (18) directly into the left-hand side of Eq. (11). If the convergence criterion is set as $|\epsilon| \le 0.01$, the dashed line in Fig. 2 shows the boundary of the region of convergence, which unfortunately is rather small.

However, the Euler transformation can be used to extend the convergent region. It is easy to show by mathematical induction that for $j \ge 2$

$$f_j(\eta) = g_j(\eta)/(\eta + b)^{2j-3}$$

where $b = 2/(1 - 2\lambda - 8\lambda^2)$ and each $g_j(\eta)$ is a polynomial of η. There is a singularity at $\eta = -b$, which can be removed by the Euler transformation

$$\eta^* = \eta/(\eta + b) \tag{19}$$

For the variable ξ, we first examine the series along the axis $\eta = 0$,

$$\phi(\xi,0) = \sum_{j=0}^{\infty} a_{j,0}\xi^j$$

The numerical results show that when j is large, the coefficients $a_{j,0}$ change sign alternatively, and behave somewhat like those of a geometric series with a singularity at a minus value of ξ. The behavior for $\eta \neq 0$ is less clear. Nevertheless, we try a similar Euler transformation

$$\xi^* = \frac{\xi \cdot h(\eta)}{1 + \xi \cdot h(\eta)} \tag{20}$$

Table 1 Coefficients $a^*_{j,k}$ of the series solution Eq. (22) for $R_T/Y_T=5$, K = 0.2

j^k	0	1	2	3	4	5	6	7	8	9
0	0.50000	1.0738	1.0938	1.1137	1.1336	1.1536	1.1735	1.1935	1.2134	1.2334
1	−0.56107	−1.6418	−3.2422	−5.3622	−8.0019	−11.161	−14.840	−19.039	−23.757	−28.995
2	−0.66527	−1.8458	−3.4329	−5.3180	−7.3925	−9.5478	−11.675	−13.666	−15.412	
3	−0.73217	−1.9496	−3.4151	−4.8599	−5.9834	−6.4533	−5.9058	−3.9455	−0.14486	
4	−0.77737	−1.9662	−3.1550	−3.8337	−3.3822	−1.0592	4.0098	12.843		
5	−0.80780	−1.9199	−2.6946	−2.2705	−0.47960	6.9999	19.108	39.058		
6	−0.82752	−1.8247	−2.0704	−0.23893	5.5236	17.750	39.829			
7	−0.83931	−1.6904	−1.3011	2.2441	11.789	31.452	67.079			
8	−0.84528	−1.5249	−0.39959	5.1906	19.436	48.775				
9	−0.84723	−1.3348	0.62406	8.6233	28.680	70.616				
10	−0.84680	−1.1267	1.7605	12.573	39.787					
11	−0.84557	−0.90747	2.9998	17.078	53.083					
12	−0.84514	−0.68450	4.3297	22.176						
13	−0.84721	−0.46630	5.7345	27.897						
14	−0.85360	−0.26262	7.1930							
15	−0.86631	−0.08518	8.6764							
16	−0.88754	0.05188								
17	−0.91976	0.13433								
18	−0.96574									
19	−1.0286									

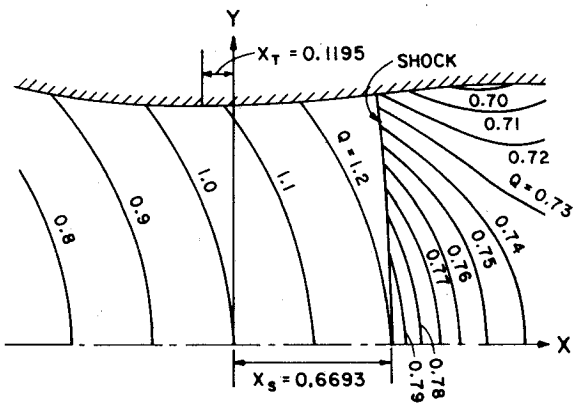

Fig. 3 Contours of constant speed and shape of nozzle after shock, for $R_T/Y_T=5$, $K=0.2$, $m=9$.

and a rough analysis suggests

$$h(\eta)=b_1(1-\eta^*)^2, \quad -b_1=\lim_{j\gg 1}\frac{a_{j,0}}{a_{j-1,0}}\doteq\frac{a_{2m+1,0}}{a_{2m,0}} \qquad (21)$$

The solution in the transformed variables is then written as [like Eq. (18)],

$$\phi=\sum_{j=0}^{2m+1}\sum_{k=0}^{m-[j/2]}a^*_{j,k}\xi^{*j}\eta^{*k} \qquad (22)$$

The coefficients $a^*_{j,k}$ with $m=9$ are listed in Table 1.

That the transformations, Eqs. (19) and (20), considerably enlarge the convergent region is shown in Fig. 2. Note that the nozzle walls are at $\eta\doteq 1$. Between the nozzle walls and in this region, we have compared the results for the perturbation speed as the number of terms in the series is changed from $m=9$ to $m=8$. The discrepancy is found to be less than 0.5%.

Fig. 3 shows the contour lines of Q, $Q\equiv\sqrt{(a^*+\Phi_X)^2+\Phi_Y^2}$ calculated with Eq. (22) and Table 1, as well as the shape of the nozzle wall behind the shock, which is determined by numerical integration of Eq. (3) using the Runge-Kutta method. Conservatively, we limit our representation to $X<1.4$, where the convergence criterion $|\epsilon|=0.01$ is first met at the wall. Although by construction the wall slope is continuous, the curvature of the nozzle wall from the present solution is, as may be expected, discontinuous at the juncture of the wall and the shock. For the example shown, the radius of curvature is 6.337 just before the shock, and −4.861 just after the shock. This discontinuity of curvature arises from the requirements of a parabolic shock shape and an analytic solution behind the shock. Note that the special shock shape produces behind the shock a flow that decelerates at first, but soon accelerates locally near the wall.

References

[1] Hall, I.M. and Sutton, E.P., "Transonic Flow in Ducts and Nozzles: A Survey," *Transactions of Symposium Transonicum*, Aachen, Sept. 1962, edited by K. Oswatitch, Springer-Verlag, Berlin, 1964, pp. 325-344.

[2] Guderley, K.G., *The Theory of Transonic Flow*, Addison-Wesley, Reading, Mass., 1962.

AIAA 81-4302

Mean Values of Unsteady Oscillations in Transonic Flow Calculations

G. David Kerlick* and David Nixon†
Nielsen Engineering and Research, Inc., Mountain View, Calif.

Introduction

In finite difference calculations of unsteady, oscillatory transonic flows about airfoils, it is observed that unsteady quantities oscillate about mean values which are different from their initial steady values. This is true of the shock positions on the upper and lower surfaces as well as the lift and moment coefficients. This is illustrated for the lift coefficient in Fig. 1.

The transonic indicial method[1,2] yields some insight into this phenomenon. It will be shown that a time constant characteristic of the indicial response fully accounts for this

Received Feb. 18, 1981; revision received May 28, 1981.

*Research Scientist. Member AIAA.

†Manager, Computational Fluid Dynamics Department. Associate Fellow AIAA.